Journal of Oceanography, Vol. 60, pp. 531 to 541, 2004

Influence of Coupled Rossby Waves on Primary Productivity and Tuna Abundance in the Indian Ocean

WARREN B. WHITE[1]*, KATHRYN A. GLOERSEN[2], FRANCIS MARSAC[3] and YVES M. TOURRE[4]

[1]*Scripps Institution of Oceanography, UCSD, La Jolla, CA 92037, U.S.A.*
[2]*University of California San Diego, La Jolla, CA 92037, U.S.A.*
[3]*UR 109 Thetis, IRD, La Reunion, France*
[4]*LDEO of Columbia University, Palisades, NY 10964, U.S.A.*

(Received 27 February 2003; in revised form 4 June 2003; accepted 10 July 2003)

Interannual coupled Rossby waves in the extratropical Indian Ocean propagate westward in covarying pycnocline depth, sea surface temperature, and meridional surface wind anomalies from the west coast of Australia between 15°S and 35°S, taking 3–4 years to transit the interior ocean to Madagascar. In the interior subtropical gyre, where the tuna longline catch (TLC) mainly concerns two species (albacore and bigeye), these waves have been observed to affect year-to-year changes in catch, with wave crests (troughs) in the main pycnocline associated with high (low) TLC anomalies. This suggested that tuna longline catch is associated with the entrainment of nutrient-rich pycnocline water into the photic zone and a subsequent increase in primary productivity there. Here, this hypothesis is examined within the context of SeaWiFS chlorophyll concentration (CC). We find the situation the opposite of that expected, with wave crests (troughs) in the main pycnocline associated with low (high) CC anomalies averaged over the photic zone. These results are shown to be consistent with a model relating the anomalous CC tendency to upper-layer divergence in the wave, not unlike that relating surface slicks to upper-layer divergence in internal gravity waves. Thus, the connection between interannual coupled Rossby waves and TLC in the interior subtropical gyre does not appear to derive from wave-induced modulation of the pelagic food web.

Keywords:
· Coupled Rossby waves,
· primary productivity,
· tuna abundance,
· Indian Ocean,
· interannual variability.

1. Introduction

White (2000a) recently found interannual coupled Rossby waves propagating westward across the extratropical Indian Ocean from 15° to 35°S in TOPEX-Poseidon sea level height (SLH) and National Centers for Environmental Prediction (NCEP) sea surface temperature (SST) and meridional surface wind (MSW) from 1993 to 1999. He found each variable propagating westward in fixed phase with one another at speeds ranging from 0.03 to 0.07 m s^{-1} (less than for uncoupled Rossby waves), taking 3–4 years to travel from Australia to Madagascar. In these coupled Rossby waves, warm SST anomalies overlie and are displaced to the west of high SLH anomalies and poleward MSW anomalies overlie warm SST anomalies. The former relationship is consistent with the upper ocean thermal balance, wherein the anomalous SST tendency is driven by anomalous meridional heat advection by the geostrophic flows of the coupled Rossby wave and SST anomalies are dissipated by an anomalous SST-induced sensible-plus-latent heat flux to the atmosphere. The latter relationship is consistent with the lower troposphere thermal and vorticity balances, wherein the warm SST-induced sensible-plus-latent heat flux anomalies convectively drive anomalous low-level convergence, the latter balanced by the anomalous meridional advection of planetary vorticity to yield poleward MSW anomalies (White and Chen, 2002). This covariance between warm SST and poleward MSW anomalies has been found in other instances of coupled Rossby waves observed over the extra-tropical ocean (White *et al*., 1998; White, 2000b, 2001; White and Annis, 2003). In the present study, we find these interannual coupled Rossby waves in covarying SLH, SST, and MSW anomalies also fluctuating in phase with the anomalous chlorophyll concentrations (CC) from the satellite-born Sea-Viewing Wide-Field of View Sensor (SeaWiFS).

* Corresponding author. E-mail: wbwhite@ucsd.edu

Recently, Marsac *et al.* (2004) found interannual coupled Rossby waves in the extratropical Indian Ocean exerting a significant influence on year-to-year variability in tuna longline catch (TLC) during autumn-winter (April through August). In this domain, the species of tunas caught with longline gear are albacore (*Thunnus alalunga*) and bigeye (*Thunnus obesus*) tuna, with hooks set at depths between 100 and 250 m in the upper part of the main pycnocline just below the photic zone. In marine ecosystems, these tunas are among the most efficient predators at the top of the food chain, with very high energy requirements. Thus, they generally concentrate in regions where the prey density is largest (Laurs *et al.*, 1984; Korsmeyer and Dewar, 2001). Marsac *et al.* (2004) found year-to-year variability in TLC propagating westward across the Indian Ocean in phase with interannual coupled Rossby waves, with high TLC anomalies associated with low SLH and shallow pycnocline depth anomalies. They proposed that shallow pycnocline depth anomalies in the coupled Rossby waves produce a biological enrichment of the surface well-mixed layer (and the photic zone) that benefits the tunas, their prey, and presumably other apex predators. The latter had been observed in mesoscale Rossby waves, ranging from ~200 km wavelength (Cipollini *et al.*, 2001) to ~1000 km wavelength (Mete Uz *et al.*, 2001) for periods <6 months, wherein shallow pycnocline depths are associated with larger chlorophyll concentrations (CC's).

In the present study we test the hypothesis of Marsac *et al.* (2004) by examining the influence that interannual coupled Rossby waves in the extratropical Indian Ocean exert on primary productivity inferred from CC measured remotely by SeaWiFS (e.g., Hooker and McClain, 2000). We conduct this case study over the 4 years from 1998 to 2001, when SeaWiFS data was available. This 4-year record allows one cycle of the interannual coupled Rossby wave to be examined. We find these Rossby wave crests (troughs) in the pycnocline associated with smaller (larger) chlorophyll concentrations (CC), the opposite of that found in mesoscale Rossby waves (Cipollini *et al.*, 2001; Mete Uz *et al.*, 2001). Thus, the anomalous upwelling arising from the propagation of the coupled Rossby wave across the interior subtropical gyre does not appear to transport (or entrain) nutrient-rich pycnocline water into the photic zone. With this biological process excluded from consideration, we examine the conservation of anomalous CC averaged over the photic zone, the latter presumed to be confined to the surface well-mixed layer. We find Rossby wave-induced divergence in the photic zone generating an anomalous CC tendency that is negative, as observed.

2. Data and Methods

In this study we utilize six variables from four different sources. We utilize monthly SST and MSW from NCEP and the National Center for Atmospheric Research (NCAR) reanalysis (Kalnay *et al.*, 1996) over the 9 years from 1993 to 2001. Over the global ocean, the NCEP-NCAR reanalysis incorporates the Comprehensive Ocean-Atmosphere Data Set (COADS) surface marine weather observations (Slutz *et al.*, 1985; Woodruff *et al.*, 1993) the Reynolds' SST data set (Reynolds and Marsico, 1993), and atmospheric soundings from weather ships and satellites (Kalnay *et al.*, 1996). These *in situ* and satellite data are assimilated into the NCEP-NCAR reanalysis model, made available monthly on a ~2° longitude-latitude grid extending over the globe from 1950 to 2001.

We utilize monthly SLH data from the TOPEX-Poseidon (T-P) satellite altimeter over the 9-year record from 1993 to 2001. These SLH data are remotely sensed along discrete ground tracks laid down by the satellite over the global ocean, with tracks repeated every 10 days. Subsequently, these track data are interpolated onto a 1° latitude-longitude grid each month from 60°S to 60°N (Fu *et al.*, 1994).

We utilize monthly tuna longline catch (TLC) from the extratropical Indian Ocean over the 6 years from 1993 to 1999, compiled by the Indian Ocean Tuna Commission (Marsac *et al.*, 2004). The longline is one of the principal gears used to catch tuna in the extratropical Indian Ocean. This gear operates at depths ranging from 50 to 250 meters (Hanamoto, 1987; Mizuno *et al.*, 1999) and targets adult fish with sizes greater than 1.1 m. The data set used here has TLC compiled each month over 5° latitude by 5° longitude spatial blocks. However, not all longline fishing activities are reported, thereby underestimating the total catch in the TLC dataset. Moreover, year-to-year variability in TLC represents not only changes in local concentration but also in its catchability by longline gear. Thus, we remain cautious in the interpretation of results.

We utilize the monthly chlorophyll concentrations (CC) measured by the satellite-born SeaWiFS for the 4 years from 1998 to 2001 (e.g., Hooker and McClain, 2000). The SeaWiFS was designed to monitor the color of the ocean, the latter providing the means to estimate the chlorophyll concentration (in mg m^{-3}) and primary productivity in the upper ocean. Since the extinction depth of visible light is near 30 m in the open ocean, SeaWiFS estimates CC anomalies averaged over most of the photic zone down to ~100 m depth. This photic zone is confined to the well-mixed layer extending from the sea surface to the top of the main pycnocline during most of autumn, winter, and spring.

We also utilize the 18°C isotherm depth (Z18) constructed each month over the Indian Ocean from 1993 to 2001 using the Scripps Institution of Oceanography (SIO) upper ocean temperature reanalysis (White, 1995; White

et al., 2001). The SIO reanalysis is based on all temperature profiles available at the National Oceanographic Data Center (NODC) (Levitus *et al.*, 1998a, b), interpolated onto a 2° latitude by 5° longitude grid over most of the global ocean (i.e., from 30°S to 60°N). The interpolation scheme utilizes the spatial covariance structure of upper ocean temperature variability to weight the data surrounding each grid point (White, 1995).

Prior to analysis, we interpolate the six variables onto the 2° latitude by 5° longitude grid of the Z18 data, centered at the middle of each month. Next, we computed long-term monthly means at each grid point over the 6-year record from 1993 to 1999 for the SLH, SST, Z18, and TLC variables, and over the 4-year record from 1998 to 2001 for the SLH, SST, Z18, and CC variables. Subsequently, we subtracted monthly long-term means to produce anomalies about the seasonal cycle.

Next, we low-pass filter the time sequences of monthly anomalies with a half-power point at 3 years, allowing us to focus on the interannual variability in these records (Kaylor, 1977). Prior to low-pass filtering, we applied maximum entropy spectral analysis (Andersen, 1974) to reduce loss of data at the ends of each time sequence due to filtering, and to preserve the integrity of the filter response. Thus, maximum entropy spectral coefficients were used to extend the time sequences by an amount equal to half the filter width on both ends of the record. This extension allows the half-power point criterion to be preserved in the response function, and it allows over half the variance of each signal at the end points to be faithfully represented (White, 2000a).

3. Interannual Coupled Rossby Waves in the Indian Ocean

The animation sequences of maps for interannual SLH, SST, and MSW anomalies extending across the Indian Ocean (0° to 34°S) for the 6 years from January 1993 to January 1999 (Fig. 1) display westward phase propagation in all three variables over most of the record, with variables better aligned after January 1994 than before. The wave crests and troughs exhibited in each variable are aligned in the northwest-southeast direction so that wavenumber vectors (normal to the crests and troughs) are directed westward and poleward. After 1995 the amplitudes of all three variables became more robust and better aligned with one another (that is, better coupled) than previously. The phase relationships between variables can be ascertained from the dashed reference lines (Fig. 1). Along this line, warm (cool) SST anomalies can be seen overlying high (low) SLH anomalies, and poleward (equatorward) MSW anomalies can be seen overlying warm (cool) SST anomalies. These phase relationships are consistent with those determined from coherence and phase analysis (White, 2000a). The slope of

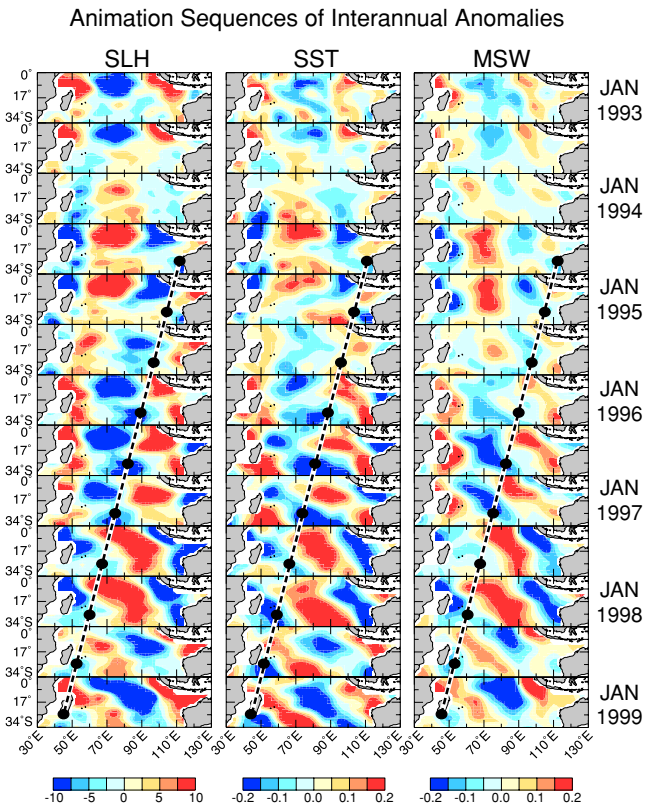

Fig. 1. Animation sequence of maps for interannual SLH, SST, and MSW anomalies over the Indian Ocean (0° to 34°S, 30°E to 130°E), displayed every 6 months from January 1993 to January 1999. Positive (negative) SLH and SST anomalies and poleward (equatorward) MSW anomalies range from yellow to red (blue to purple) colors with contour intervals of 2.5 cm for SLH anomalies, 0.05°C for SST anomalies, and 0.05 m s^{-1} for MSW anomalies. Dashed lines repeated in each animation sequence, connecting dots near 25°S, provide a reference. The sense of propagation comes from following anomalies of similar sign from one map to the next in each animation sequence of maps.

the dashed reference line yields a westward phase speed of –0.04 ± 0.01 m s^{-1} near 28°S.

These animation sequences reveal three important aspects of coupled Rossby waves in the extratropical Indian Ocean on interannual timescales. First, they are coupled more intensely during the later 2/3 of the 6-year record than during the earlier 1/3, as evidenced by the better alignment of the three variables and their higher amplitudes after mid-1994 (Fig. 1). This indicates that the coupling of the Rossby waves with the overlying atmosphere can be intermittent, more intense during some epochs than others for reasons which are not understood. This can be expected to produce epochal changes in phase speed as well. Second, these coupled Rossby waves can

be seen originating at the eastern boundary along the west coasts of Indonesia and Australia, where they appear to be pumped by the anomalous MSW along these coasts, as observed along the west coast of North America (White and Saur, 1983). Third, once formed at the eastern boundary, these Rossby wave propagate westward together with the MSW anomalies in the overlying atmosphere. The maintenance of amplitude as the coupled Rossby wave propagates westward from the eastern boundary is a consequence of an instability in the coupled wave, allowing growth to balance dissipation in the wave (White and Annis, 2003). Recently, Potemra (2001) found interannual Rossby waves emanating from the northwest coast of Australia stemming from Kelvin waves propagating poleward from the equator, driven by zonal winds in the western equatorial Pacific Ocean. It remains to be determined whether the interannual MSW anomalies along the boundary are instigated by Kelvin wave-induced coastal upwelling/downwelling.

4. Statistics of Tuna Longline Catch and Chlorophyll Concentration

We begin by displaying the distribution of mean TLC and CC, and the RMS of the interannual TLC and CC anomalies over the extra-tropical Indian Ocean, the former computed over the 6 years from 1993 to 1999 and the latter computed over the 4 years from 1998 to 2001 (Fig. 2). The sources of these two data sets allow these statistics to overlap by only one year. The distribution of mean TLC is maximum near 32°S (Fig. 2(a)), but this maximum runs parallel to the gyre's poleward and eastward limbs as defined by the horizontal distribution of mean pycnocline density (Peixoto and Oort, 1992, p. 193). This is consistent with the report by Laurs *et al.* (1984), who found tuna to be visual feeders, hunting their prey in the clear water of the interior subtropical gyre but near fronts where prey is concentrated. Presumably, the presence of tuna prey is enhanced by increased primary productivity in the photic zone, with energy transferred from first to intermediate levels in the food web. Thus, it comes as no surprise to find the distribution of maximum mean TLC (Fig. 2(a)) aligned parallel to the interior edge of maximum mean CC along the poleward and eastward limbs of the subtropical gyre (Fig. 2(b)). The RMS of both interannual TLC and CC anomalies (Figs. 2(c) and (d)) can be seen to overlay the mean TLC and CC, respectively. This relationship is consistent with interannual anomalies arising from the anomalous horizontal advection and/or the anomalous divergences/convergences in the mean state.

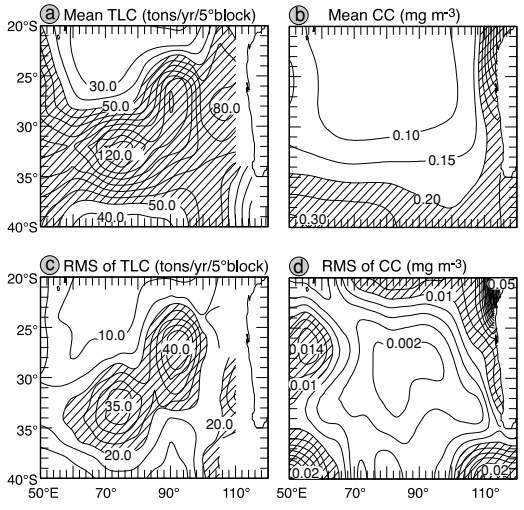

Fig. 2. Distributions of mean TLC (a) and CC (b) over the Indian Ocean, together with those of their interannual RMS variability ((c) and (d), respectively). The mean and RMS variability of TLC is computed over the 6 years from 1993 to 1999, while that for CC is computed over the 4 years from 1998 to 2002. Hatching is for effect. Contours of mean TLC and CC are 10 tons per year per 5° block and 0.05 mg m^{-3}, respectively, while those for the RMS of interannual TLC and CC anomalies are 5 tons per year per 5° block and 0.0025 mg m^{-3}.

5. Influence of Interannual Coupled Rossby Waves on Tuna Longline Catch

Now we introduce our plotted animation sequences of maps for interannual SLH, Z18, and TLC anomalies across the Indian Ocean (20°S to 40°S) for the 6 years from June 1993 to June 1999 (Fig. 3). This figure displays westward phase propagation of the coupled Rossby wave in all three variables over most of the record, the waves initiated at the west coast of Australia and taking 3 to 4 years to transit the Indian Ocean. The phase relationships among the three variables can be discerned qualitatively by the dashed reference lines repeated in each animation sequence (Fig. 3). Along these dashed lines, low SLH anomalies can be seen aligned with or displaced to the west of shallow Z18 anomalies, with high TLC anomalies generally overlying shallow Z18 anomalies.

To confirm quantitatively the zonal phase relationships among the three variables, we plot time-longitude diagrams of interannual SLH, Z18, and TLC anomalies from 70°E to 110°E along 28°S for the 6 years from 1993 to 1999 (Fig. 4(a)). The sloping black line, repeated in each diagram, is aligned with the coupled Rossby wave trough in Z18 anomaly, which usually corresponds to a crest in SLH anomaly (see Section 7 below). It yields a westward phase speed of -0.03 ± 0.01 m s^{-1}, the same as for the sloping dashed line in Fig. 3. Using this sloping black line as a reference, we observe high TLC anoma-

lies propagating westward together with shallow Z18 anomalies, with low SLH anomalies occurring directly over shallow Z18 anomalies east of 90°E, but displaced nearly 90° of phase west of 95°E. This is confirmed by the zonal-lag cross-correlation between interannual Z18 anomalies and interannual SLH and TLC anomalies (Fig. 4(b)). This alignment of high TLC anomalies with shallow Z18 anomalies in these interannual coupled Rossby wave is consistent with that observed by Marsac *et al.* (2004).

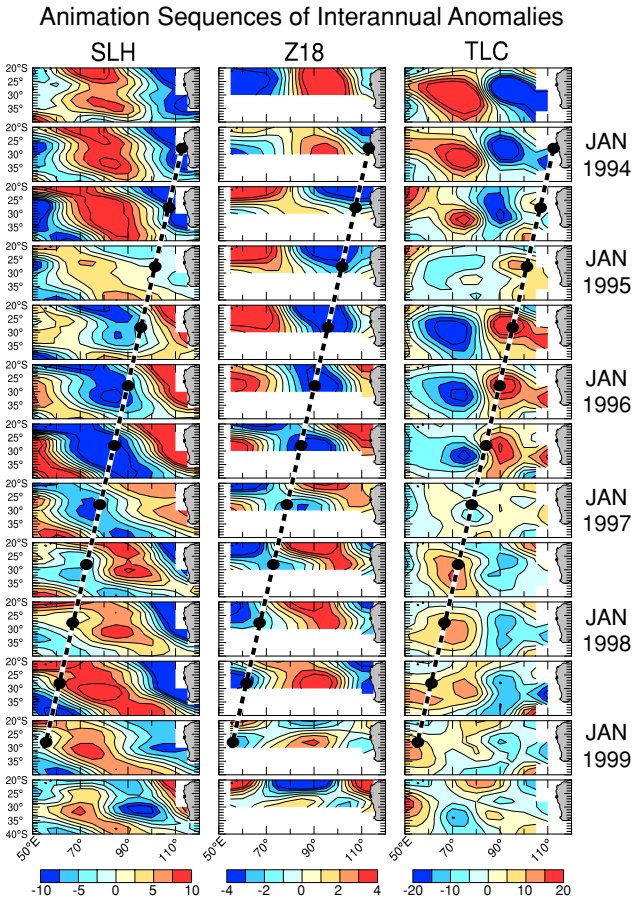

Fig. 3. Animation sequences of maps for interannual SLH, Z18, and TLC anomalies over the subtropical gyre in the Indian Ocean (20°S to 40°S, 50°E to 120°E), displayed every 6 months from June 1993 to June 1999. Positive (negative) SLH, Z18, and TLC anomalies range from yellow to red (blue to purple) colors, with contour intervals of 2.5 cm for SLH anomalies, 1.0 m for Z18 anomalies, and 5 tons per year per 5° block for TLC anomalies. Dashed lines are repeated in each animation sequence, connecting the dots near 28°S and providing a reference. The sense of propagation comes from following anomalies of similar sign from one map to the next in each animation sequence of maps.

6. Influence of Interannual Coupled Rossby Waves on Chlorophyll Concentration

Next, we plot animation sequences of maps for interannual SLH, Z18, and CC anomalies across the Indian Ocean (20°S to 40°S) for the 4 years from January 1998 to June 2001 (Fig. 5). This figure displays the westward phase propagation of the coupled Rossby wave in all three variables over the 4-year record, with waves initiated at the west coast of Australia and taking 3 to 4 years to transit the Indian Ocean. The phase relationships between variables can be discerned qualitatively from the sloping dashed reference line repeated in each animation sequence (Fig. 5). Along these dashed lines, low SLH anomalies can be seen overlying or displaced to the west of shallow Z18 anomalies, with low CC anomalies generally overlying shallow Z18 anomalies.

To confirm quantitatively the phase relationships among the three variables, we have plotted time-longitude diagrams of interannual SLH, Z18, and CC anoma-

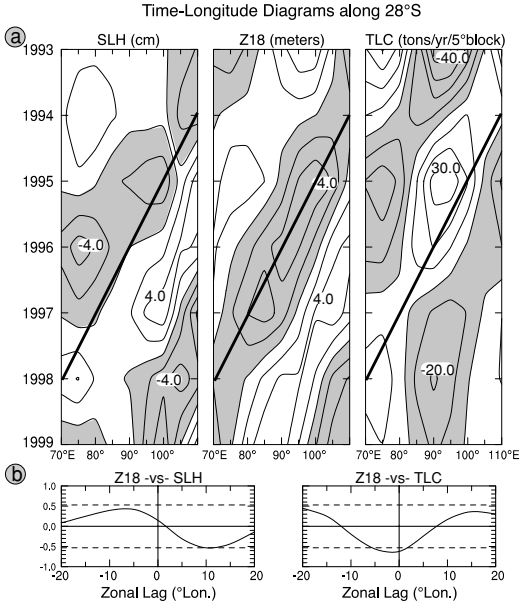

Fig. 4. (a) Time-longitude diagrams of interannual SLH, Z18 and TLC anomalies across the Indian Ocean from 70°E to 110°E at 28°S from 1963 to 1999. Positive (negative) anomalies are unshaded (shaded). Sloping dashed lines repeated in each diagram allow the alignment of westward phase propagation among the 3 variables to be realized. Contours intervals for SLH, Z18, and TLC anomalies are 2 cm, 2 m and 10 tons per year per 5° block. (b) Zonal-lag cross-correlations between Z18 and SLH anomalies and between Z18 and TLC anomalies, with 90% confidence limits given by the horizontal dashed lines for 6 effective degrees of freedom respectively (Snedecor and Cochran, 1980).

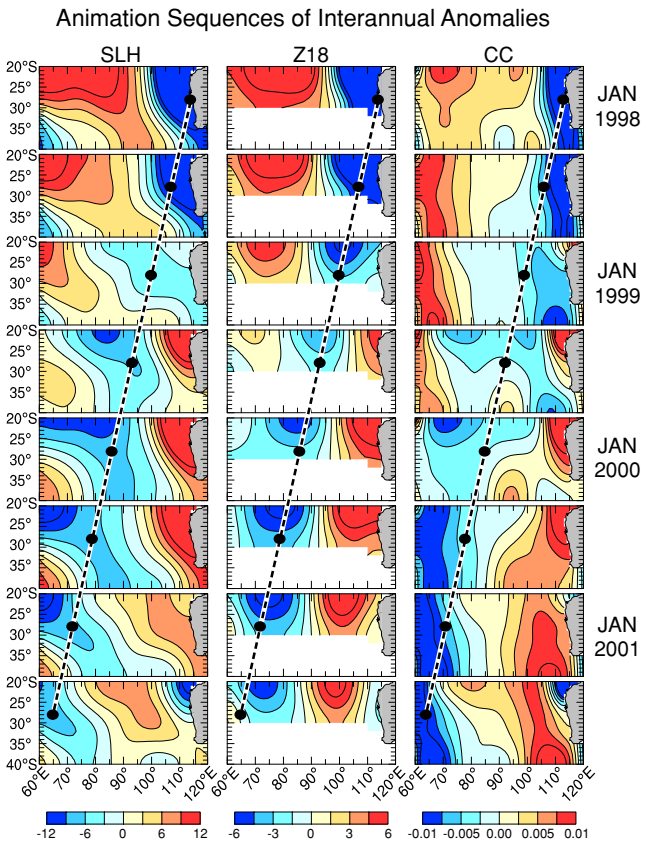

Fig. 5. Animation sequence of maps for interannual SLH, Z18, and CC anomalies over the subtropical gyre in the Indian Ocean (20°S to 40°S, 60°E to 120°E), displayed every 6 months from January 1998 to June 2001. Positive (negative) SLH, Z18, and CC anomalies range from yellow to red (blue to purple) colors, with contour intervals of 3 cm for SLH anomalies, 1 m for Z18 anomalies, and 0.0025 mg m^{-3} for CC anomalies. Dashed lines are repeated in each animation sequence, connecting the dots near 28°S and providing a reference. The sense of propagation comes from following anomalies of similar sign from one map to the next in each animation sequence of maps.

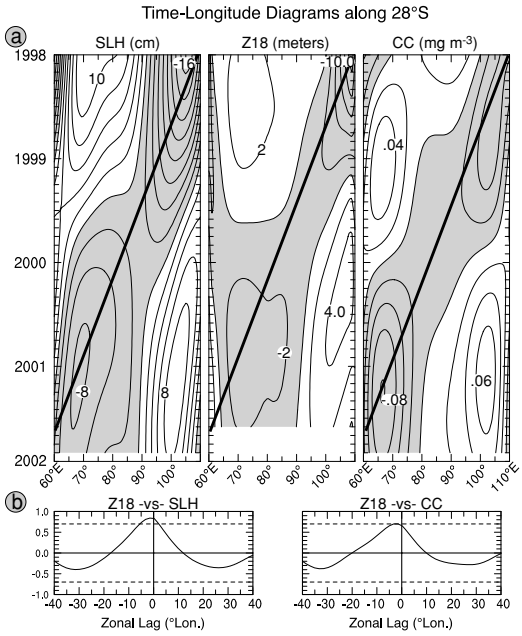

Fig. 6. (a) Time-longitude diagrams of interannual SLH, Z18 and CC anomalies across the Indian Ocean from 60°E to 110°E at 28°S from 1998 to 2002. Positive (negative) anomalies are unshaded (shaded). Sloping dashed lines repeated in each diagram allow the alignment of westward phase propagation among the 3 variables to be realized. Contours intervals for SLH, Z18, and CC anomalies are 2.0 cm, 2 m, and 0.02 mg m^{-3}. (b) Zonal-lag cross-correlations between Z18 and SLH anomalies and between Z18 and CC anomalies, with 90% confidence limits given by the horizontal dashed lines for 6 effective degrees of freedom respectively (Snedecor and Cochran, 1980).

lies from 60°E to 110°E along 28°S for the 4 years from January 1998 to December 2001 (Fig. 6(a)). The sloping black line, repeated in each diagram, is aligned with the Rossby wave trough in Z18 anomaly. This yields a westward zonal phase speed of –0.04 ± 0.01 m s^{-1}, the same as for the sloping dashed line in Fig. 5. Using this sloping black line as a reference, we observe low CC anomalies propagating westward together with shallow Z18 anomalies, with low SLH anomalies aligned with shallow Z18 anomalies. This is confirmed by the zonal-lag cross-correlation between interannual Z18 anomalies and interannual SLH and CC anomalies (Fig. 6(b)). This relationship between Z18 and CC anomalies is the opposite of that observed in both small and large mesoscale Rossby waves of intra-annual period (Cipollini *et al.*, 2001; Mete Uz *et al.*, 2001). This indicates that the process of upwelling and/or entrainment of nutrient-rich pycnocline water into the surface well-mixed layer above interannual Rossby wave crests does not operate in the interior subtropical gyre of the Indian Ocean.

7. Vertical Section of Interannual Coupled Rossby Wave Propagation

To determine the vertical depth scale of the interannual Rossby waves propagating westward in the main pycnocline of the extratropical Indian Ocean, we have constructed an animation sequence of vertical sections of interannual upper ocean temperature anomalies for the 8 years from June 1993 to June 2001 (Fig. 7). In this animation sequence, each section extends vertically from the sea surface to 400 m depth and zonally from 60°E to 110°E. The upper ocean temperature anomalies are meridionally averaged from 24°S to 28°S in order to

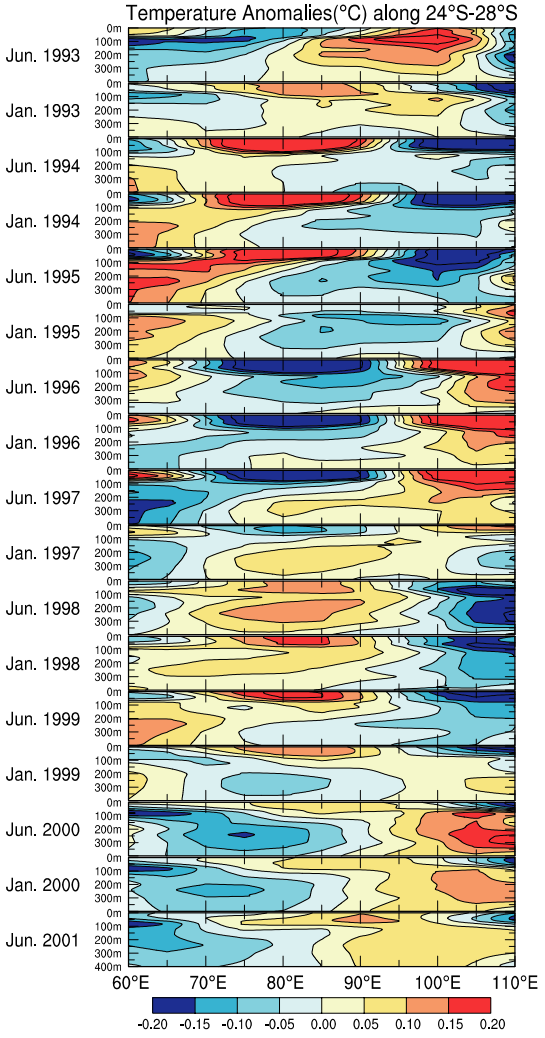

Fig. 7. Animation sequence of the vertical section of interannual temperature anomalies for 8-years from 1993 to 2001, each vertical section extending from the surface to 400 m depth and zonally along 28°N from 60°E to 110°E. Positive (negative) temperature anomalies range from yellow to red (blue to purple) colors, with contour intervals of 0.2°C cm. The sense of propagation comes from following anomalies of similar sign from one section to the next in the animation sequence.

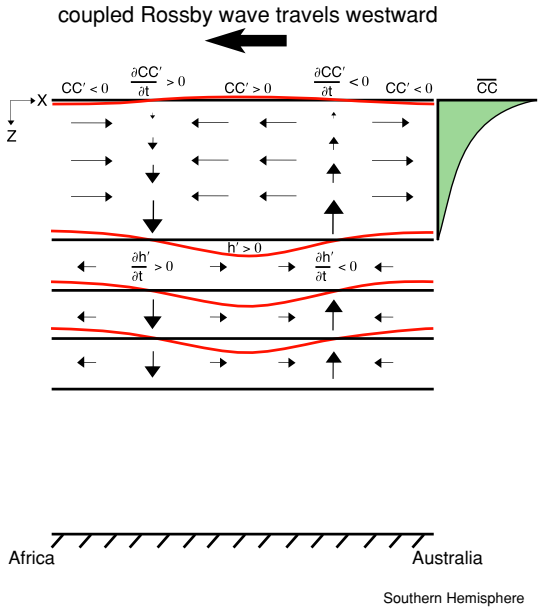

Fig. 8. Schematic diagram illustrating the influence that coupled Rossby waves have on chlorophyll concentrations (CC) in the interior subtropical gyre of the Indian Ocean, where horizontal mean CC gradients are weak but vertical mean CC gradients are robust. The Rossby wave travels westward in the negative *x*-direction, with a crest in sea level height (i.e., the red line at the sea surface) associated with a trough in pycnocline depth (the red lines in the main pycnocline). The Rossby wave is an internal wave in the main pycnocline, with sea level height anomalies responding to changes in the thickness of upper layer of uniform density. The horizontal and vertical flow vectors indicate the relatively weak divergent flows of the Rossby wave. The vertical velocity is maximum at the top of the main pycnocline and decreases linearly to zero at the sea surface. The anomalous CC tendency, $\partial CC'/\partial t$, occurs at the same longitude as the anomalous pycnocline depth tendency, $\partial h'/\partial t$, as a consequence of the anomalous vertical advection of the mean CC, the latter maximum at the sea surface and decreasing exponentially with depth. This upper-layer divergent (convergent) motion is balanced by correspondingly weaker convergent (divergent) motion spread over the main pycnocline, diminishing into the deep ocean below.

smooth the result. This record length spans the intercomparison of SLH, Z18, and TLC anomalies from 1993 to 1999 (Figs. 3 and 4) and the intercomparison of SLH, Z18, and CC anomalies from 1998 to 2001 (Figs. 5 and 6).

In this animation sequence we find the Rossby waves in interannual upper ocean temperature anomalies propagating westward from the west coast of Australia, taking 3-to-4 years to transit the section, consistent with the waves displayed in Figs. 3 and 5. The wave propagation can be seen to occur near 100 m depth at 110°E, extending from 100 to 300 m at 85°E, and extending from 100 to 400 m at 60°E. Superimposed on this propagation is a standing wave component of upper ocean temperature variability in the upper 100 m near the middle of the section, which was quite intense during the first half of the record but much weaker during the second half. The later conditions allowed the Rossby wave propagation at mid-depth to be recognized more easily.

Earlier, we found the zonal phase lag between SLH and Z18 anomalies from 1993 to 1999 (Fig. 4(b)) to be different from that observed from 1998 to 2002 (Fig. 6(b)),

with the 90° phase difference west of 90°E during the earlier period disappearing after 1997. From inspection of the animation sequence of anomalous upper ocean temperature sections (Fig. 7), this secular change can be explained in the following way. Interannual SLH anomalies are mostly thermosteric, arising from temperature anomalies integrated over the column. The latter has two principal sources: (1) vertical displacements in the main pycnocline from baroclinic Rossby waves (i.e., effecting adiabatic thermosteric changes in SLH); and (2) heat storage changes in the upper layer accompanying SST anomalies (i.e., effecting diabatic thermosteric changes in SLH). In the upper ocean west of 90°E (Fig. 7), we find the intense standing wave component of upper ocean temperature anomaly during the first half of the record contributing more to the thermosteric SLH anomalies than do the pycnocline temperature anomalies arising from the Rossby wave propagation at mid-level. Thus, SLH anomalies are decoupled from the Z18 anomalies over the western ocean during the first half of the record. But during the second half of the record they mimic the behavior of Z18 anomalies.

8. Conserving Chlorophyll Concentration in the Presence of Interannual Coupled Rossby Waves

Now we consider the conservation equation for anomalous chlorophyll concentration in the upper layer of the ocean within the context of interannual coupled Rossby waves in the absence of biological sources and sinks i.e.:

$$\partial CC'/\partial t = -V_H\cdot(\nabla_H CC') - V_H'\cdot(\nabla_H CC) + w'(CC/H), \quad (1)$$

where CC and CC' are the mean and anomalous chlorophyll concentration (mg m^{-3}) averaged over the upper layer, respectively; and V_H and V_H' are the mean and anomalous horizontal velocity vectors averaged over the upper layer, respectively; and w' is the anomalous vertical velocity averaged over the upper layer (i.e., $w' = 0.5\partial h'/\partial t$) arising from the propagation of the interannual Rossby wave in the main pycnocline below, as illustrated in the schematic diagram (Fig. 8). In the upper layer, the vertical velocity is maximum at the top of the pycnocline (i.e., $\partial h'/\partial t$), positive downward, decreasing to zero at the sea surface, associated with anomalous divergence in the upper layer (i.e., $\partial h'/\partial t = -H\nabla\cdot V_H'$). While SeaWiFS measures the average CC in the photic zone, the mean CC has a vertical profile that is maximum near the sea surface and decreases exponentially with depth, as illustrated in Fig. 8. This profile follows the extinction of visible sunlight with depth (Parsons *et al*., 1990, p. 94). It yields a vertical gradient of mean CC in the upper layer that is scaled as $(2CC/H)$. Thus, the CC' tendency on the left-hand-side of Eq. (1) is balanced on the right-hand-side by the sum of the mean horizontal advection of CC– by V_H, the residual horizontal advection of CC by V_H', and the residual vertical advection of CC by w', with the mean vertical velocity assumed to be zero throughout the column.

We have ignored biological sources and sinks of the CC' tendency in Eq. (1), allowing CC' to be treated as a conserved quantity. A source/sink term could have been included, representing changes in primary productivity occurring in response to the anomalous upwelling/downwelling of nutrient-rich pycnocline water into the upper layer through the passage of the interannual Rossby wave. This would allow a growth term (KCC') to be added to the right-hand-side of Eq. (1), taking the form $-K(CC/H)h'$, where h' is the anomalous depth of the main pycnocline and K^{-1} is the e-folding time scale for growth in chlorophyll concentration. In this case, a Rossby wave crest (i.e., $h' < 0$) would produce a positive CC' tendency on the left-hand-side of Eq. (1) in response to the nutrient-rich water penetrating into the upper layer. In the coastal zone and near open ocean fronts, a biological source/sink term of this kind is appropriate since upwelling is known to transport nutrient-rich pycnocline water into the upper layer (Parsons *et al*., 1990, p. 30). Based on this conventional wisdom and its validation in mesoscale Rossby waves of intra-annual period (Cipollini *et al*., 2001; Mete Uz *et al*., 2001), Marsac *et al*. (2004) proposed that the upwelling associated with interannual Rossby waves in the interior subtropical gyre likewise transports nutrient-rich pycnocline water into the upper layer, providing the simplest explanation for the association between positive (negative) TLC anomalies and Rossby wave crests (troughs). However, the Marsac *et al*. (2003) hypothesis in the interior subtropical gyre has already been rejected by observing the association between negative (positive) CC' and Rossby wave crests (troughs) (Fig. 6). This means that vertical displacements of the main pycnocline of ~5 m per year by the passage of interannual Rossby waves across the interior subtropical gyre of the Indian Ocean are unable to transport (or instigate the entrainment of) nutrient-rich pycnocline water into the upper layer. Thus, we resort to explaining the observed phase relationship between CC' and pycnocline depth anomalies in purely dynamic terms (Eq. (1)).

The conservation of vorticity in the upper layer of the ocean on spatial scales much larger than the Rossby radius of deformation yields the long Rossby wave equation (e.g., Pedlosky, 1987); i.e.,

$$\beta v' = -f(\nabla_H\cdot V') = (f/H)\partial h'/\partial t, \quad (2)$$

where v' is the anomalous meridional component of horizontal velocity; β is the meridional gradient of Coriolis

parameter (f), and h′ is the anomalous depth of the main pycnocline, positive downward. This Rossby wave equation is not coupled to the atmosphere, nor does it need to be for our present purposes. However, in future studies the coupling may be found to have an impact on the conservation of CC′ in the upper layer of the ocean through the turbulent exchange of heat and mechanical energy with the atmosphere across the air-sea interface.

We now combine the two conservation equations (i.e., Eqs. (1) and (2)), making a simplifying assumption that $\nabla_H \cdot CC \approx \partial CC/\partial y$ and $V_H \approx 0$ in the interior subtropical gyre. This yields

$$\partial CC'/\partial t = v'[(f^{-1})\partial f/\partial y - (CC^{-1})\partial CC/\partial y](CC), \quad (3)$$

where the CC′ tendency on the left-hand-side of Eq. (3) is balanced on the right-hand-side by the sum of the anomalous meridional advection of *CC* and the anomalous meridional advection of planetary vorticity in the presence of *CC*. Thus, the upper-layer meridional geostrophic velocity component in the coupled Rossby wave not only contributes to the CC′ tendency through anomalous meridional advection of the background gradient of *CC*, but also through the anomalous convergence/divergence in the upper layer in the presence of the exponential profile of *CC* with depth (Fig. 8).

When we substitute a wave form (i.e., $\exp(i(kx - \sigma t))$) for CC′ and h′ into Eq. (3), where $v' = (g'/f)\partial h'/\partial x$, this allows the amplitudes of the waves (CC_O' and h_O') to be related; i.e.,

$$CC_O' = -[(CC)[(f^{-1})\partial f/\partial y - (CC^{-1})\partial CC/\partial y](g'/f)(k/\sigma)]h_O'. \quad (4)$$

Because $f < 0$ in the southern hemisphere, $\partial CC/\partial y < 0$ in the interior subtropical gyre, and $(k/\sigma) < 0$ for westward propagating Rossby waves, the two terms in brackets on the right-hand side of Eq. (4) are of opposite sign, tending to cancel. Thus, where the divergence term (i.e., $(f^{-1})\partial f/\partial y$) dominates on the right-hand side of Eq. (4), CC_O' and h_O' fluctuates in phase with one another. But where the advection term (i.e., $(CC^{-1})\partial CC/\partial y$) dominates, CC_O' and h_O' fluctuate out of phase with one another.

We compute the coefficient linking CC_O' and h_O' in Eq. (4) (i.e., $-f^{-1}\partial f/\partial y + CC^{-1}\partial CC/\partial y$)) over the extratropical Indian Ocean from 20°S to 40°S (Fig. 9(a)) based on the distribution of *CC* already displayed (Fig. 2(b)). This distribution shows the linking coefficient to be positive (i.e., $(f^{-1})\partial f/\partial y > (CC^{-1})\partial CC/\partial y$) over most of the interior subtropical gyre, including along most of the 28°S section except near the middle of the gyre. On the other hand, near the poleward limb of the subtropical gyre at 36°S the linking coefficient is negative (i.e., $(CC^{-1})\partial CC/\partial y > (f^{-1})\partial f/\partial y$). We test this result by examining time-longitude diagrams of interannual CC and SLH anomalies, the latter acting as a surrogate for Z18 anomalies from 1998 to 2002 along both 28°S and 36°S in the Indian Ocean (Fig. 9(b)). These time-longitude diagrams and corresponding zonal-lag cross-correlations (Fig. 9(c)) show interannual CC and SLH anomalies cross-correlated positively in the interior subtropical gyre (where the linking coefficient is positive) and cross-correlated negatively near the poleward limb of the subtropical gyre (where the linking coefficient is negative), as expected from Eq. (4).

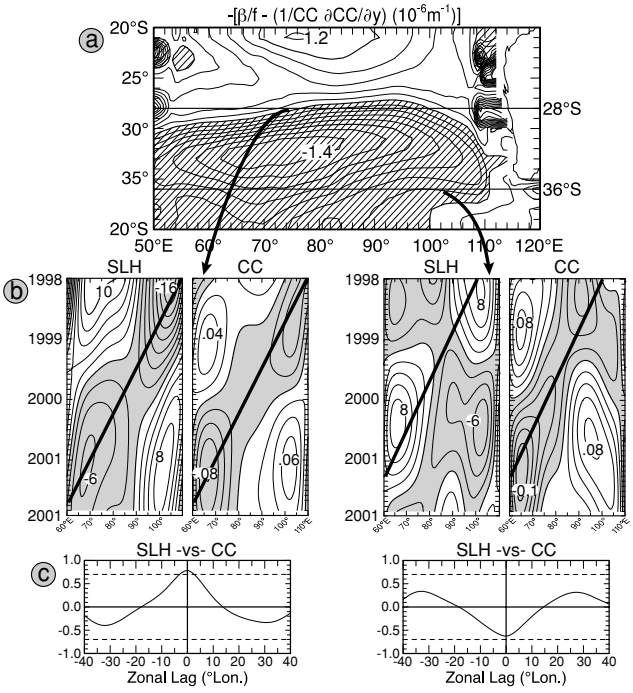

Fig. 9. (a) Distribution of the linking coefficient (i.e., $-(f^{-1}\partial f/\partial y - CC^{-1}\partial CC/\partial y)$) in Eq. (4) over the subtropical gyre of the Indian Ocean from 20°S to 40°S and 50°E to 120°E, with a contour interval of 0.25×10^{-6} m^{-1}. Positive (negative) estimates are unshaded (shaded). (b) Time-longitude diagrams of interannual SLH and CC anomalies across the Indian Ocean from 60°E to 110°E at 28°S (left) and 36°S (right) from 1998 to 2002. Positive (negative) anomalies are unshaded (shaded). SLH (CC) anomalies are in units of cm (mg/m^{-3}). (c) Zonal-lag cross-correlations between SLH and CC anomalies at 28°S (left) and 36°S (right), with 90% confidence limits given by the horizontal dashed lines for 6 effective degrees of freedom respectively (Snedecor and Cochran, 1980).

9. Discussion and Conclusions

We have found interannual coupled Rossby waves propagating westward across the extratropical the Indian Ocean over the 9 years from 1993 to 2001. These waves

emanate from the west coast of Australia, taking 3-to-4 years to transit the interior ocean to the longitude of Madagascar. In the interior subtropical gyre, we find these coupled Rossby waves influencing year-to-year changes in tuna longline catch, with Rossby wave crests (troughs) in the main pycnocline associated with high (low) catch anomalies, as observed by Marsac *et al.* (2004). Earlier, Marsac *et al.* (2004) proposed that this relationship stems from the transport of nutrient-rich pycnocline water into the upper layer through anomalous upwelling introduced by the passage of interannual Rossby waves in the main pycnocline. They expected to find shallow (deep) pycnocline depth anomalies associated with more (less) primary productivity (or chlorophyll concentration), as observed already in mesoscale Rossby waves of intra-annual period by Cipollini *et al.* (2001) and Mete Uz *et al.* (2001). This hypothesis was predicated on the basis of the belief that greater TLC should coincide with enhancement of the pelagic food web.

We tested the Marsac *et al.* (2004) hypothesis by examining year-to-year changes in chlorophyll concentration in the context of these interannual coupled Rossby waves. Unfortunately, we did not have CC and TLC datasets overlapping to any significant degree, so we could only link the two variables to SLH and Z18 anomalies over their respective periods of availability; i.e., 1993 to 1999 for TLC and 1998 to 2002 for CC. During the latter epoch, positive (negative) CC anomalies in the upper layer were associated with Rossby wave troughs (crests) in the main pycnocline, the opposite of that observed in Rossby waves by Cipollini *et al.* (2001) and Mete Uz *et al.* (2001). Thus, we were left to explain the observed phase relationship between CC and pycnocline depth anomalies in purely dynamic terms, neglecting the biological sources/sinks of primary productivity.

So we proposed a purely dynamical model to explain how interannual coupled Rossby wave crests and troughs in the main pycnocline generate weak and strong interannual CC anomalies, respectively, in the surface well-mixed layer. We examined the theoretical CC budget of the upper ocean in the absence of sources and sinks. We found it driven principally by anomalous meridional advection of the background meridional CC gradient by the anomalous geostrophic flow of the Rossby waves and by the anomalous vertical advection of the mean vertical CC gradient in the photic zone associated with anomalous divergence and convergence in the upper layer accompanying the coupled Rossby waves. We found the anomalous vertical advection dominating in the interior subtropical gyre where the mean meridional CC gradients are relatively weak and the mean vertical CC gradients are assumed to be relatively strong. This mechanism produces the observed phase relationship between coupled Rossby wave crests and troughs in the main pycnocline, and weak and strong CC anomalies, respectively, in the surface well-mixed layer above it. The behavior of this mechanism is analogous to that of producing surface slicks in response to divergences and convergences of internal gravity waves in the near-shore environment. On the other hand, we found the anomalous meridional geostrophic advection dominating near the poleward limb of the subtropical gyre where the mean meridional CC gradients are relatively strong. The latter mechanism produces the observed phase relationship between coupled Rossby wave crests and troughs in the main pycnocline and strong and weak CC anomalies, respectively. This latter phase relationship is the same as that observed in mesoscale Rossby waves by Cipollini *et al.* (2001) and Mete Uz *et al.* (2001), but it may occur for different reasons.

To test this model, we computed the coefficient linking CC and SLH anomalies in the model budget, finding the linking coefficients to be positive over most of the interior subtropical gyre and negative over the poleward limb of the subtropical gyre. Next, we constructed time-longitude diagrams of interannual SLH and CC anomalies over these positive and negative linking coefficients. Indeed, we found the observed phase relationship between SLH and CC anomalies to be positive (negative) where the linking coefficients are positive (negative). This provided an explanation for the influence that interannual coupled Rossby waves exert on chlorophyll concentration in the two sub-regions of the subtropical gyre. In the interior subtropical gyre, Rossby wave divergence dominates, increasing (decreasing) the chlorophyll concentration over deep (shallow) pycnocline depth anomalies. Near the poleward limb of the subtropical gyre, Rossby wave geostrophic advection dominates, increasing (decreasing) the chlorophyll concentration over shallow (deep) pycnocline depth anomalies.

The interannual variability in TLC in the interior subtropical gyre of the Indian Ocean occurs below the photic zone in the main pycnocline at depths of 100 to 250 m, with year-to-year variability occurring out of phase with CC in the photic zone. This result indicates that the connection between Rossby waves and tuna longline catch observed in the interior subtropical gyre by Marsac *et al.* (2003) does not derive from some simple wave-induced modulation of the pelagic food web.

Acknowledgements

Appreciation is extended to Arthur (Ted) Walker, the programmer responsible for the analyses conducted in this study. We extend our thanks to Andrea Fincham who is responsible for drafting the figures displayed in this study. Warren White is supported by Office of Global Programs of NOAA (NOAA NA 17RJ1231) under the Experimental Climate Prediction Center and by the National Aero-

nautics and Space Administration (NASA) under contract NAG5-12465. Warren White is also supported by the Scripps Institution of Oceanography of the University of California San Diego in La Jolla. Kathryn Gloersen is supported by Center for Mathematic and Science Education, a joint program between the University of California San Diego and the San Diego State University. Francis Marsac is supported by the Institut de Recherche pour le Développement (IRD), Paris, France. Yves Tourre is supported by Lamont-Doherty Earth Observatory (LDEO) at Columbia University in New York.

References

Andersen, N. (1974): On the calculation of filter coefficients for maximum entropy spectral analysis. *Geophysics*, **39**, 69–72.

Cipollini, P., D. Cromwell, P. G. Challenor and S. Raffaglio (2001): Rossby waves detected in global ocean colour data. *Geophys. Res. Lett.*, **28**, 323–326.

Fu, L.-L., E. J. Christensen, C. Y. Yamarone, M. Lefebvre, Y. Menard, M. Dorrer and P. Escudier (1994): TOPEX/POSEIDON mission overview. *J. Geophys. Res.*, **99**, 24369–24381.

Hanamoto, E. (1987): Effect of oceanographic environment on bigeye tuna distribution. *Bull. Japan. Soc. Fish. Oceanogr.*, **51**, 203–216.

Hooker, S. and C. McClain (2000): The calibration and validation of SeaWiFS data. *Prog. Oceanogr.*, **45**, 427–465.

Kalnay, E. and co-authors (1996): The NCEP/NCAR 40-year reanalysis project. *Bull. Amer. Meteorol. Soc.*, **77**, 437–471.

Kaylor, R. E. (1977): Filtering and decimation of digital time series. Inst. Phys. Sci. and Tech., Univ. of Maryland, College Park. Tech Rept. Note BN 850, 14 pp.

Korsmeyer, K. E. and H. Dewar (2001): Tuna metabolism and energetics. p. 35–78. In *Fish Physiology*, Vol. 19, ed. by B. A. Block and E. D. Stevens, Academic Press.

Laurs, R. M., P. C. Fiedler and D. R. Montgomery (1984): Albacore tuna catch distributions relative to environmental features observed from satellites. *Deep-Sea Res.*, **31**, 1085–1099.

Levitus, S., T. P. Boyer, M. E. Conkright, T. O'Brien, J. Antonov, C. Stephens, L. Stathoplos, D. Johnson and R. Gelfeld (1998a): *World Ocean Database 1998 Volume 1: Introduction*. NOAA Atlas NESDIS 18, U.S. Government Printing Office, Washington, D.C.

Levitus, S., T. P. Boyer, M. E. Conkright, D. Johnson, T. O'Brien, J. Antonov, C. Stephens and R. Gelfeld (1998b): *World Ocean Database 1998 Volume 2: Temporal Distribution of Mechanical Bathythermograph Profiles*. NOAA Atlas NESDIS 19, U.S. Government Printing Office, Washington, D.C.

Marsac, F., W. B. White and Y. M. Tourre (2004): Coupling of tuna catch and planetary waves on interannual timescales in the Indian Ocean. *Fish. Oceanogr.* (in review).

Mete Uz, B., J. A. Yoder and V. Osychny (2001): Pumping of nutrients to ocean surface waters by the action of propagating planetary waves. *Nature*, **409**, 597–600.

Mizuno, K., M. Okazaki, H. Nakano and H. Okamura (1999): Estimating the underwater shape of tuna longlines with micro-bathythermographs. *Inter-American Tropical Tuna Commission, Special Rep.*, **10**, 35 pp.

Parsons, T. R., M. Takahashi and B. Hargrave (1990): *Biological Oceanographic Processes*. Pergamon Press, 330 pp.

Pedlosky, J. (1987): *Geophysical Fluid Dynamics*. Springer-Verlag, 710 pp.

Peixoto, J. P. and A. H. Oort (1992): *Physics of Climate*. Amer. Inst. of Physics Press, Woodbury, N.Y., 520 pp.

Potemra, J. T. (2001): Contribution of equatorial Pacific winds to southern tropical Indian Ocean Rossby waves. *J. Geophys. Res.*, **106**, 2407–2422.

Reynolds, R. W. and D. C. Marsico (1993): An improved real-time global sea surface temperature analysis. *J. Climate*, **6**, 114–119.

Slutz, R. J., S. J. Lubker, J. D. Hiscox, S. D. Woodruff, R. L. Jenne, D. H. Joseph, P. M. Steurer and J. D. Elms (1985): *Comprehensive Ocean-Atmosphere Data Set; Release 1*. NOAA Environmental Research Lab., Boulder, CO, 268 pp.

Snedecor, G. W. and W. G. Cochran (1980): *Statistical Methods*. Iowa State Univ. Press, Ames, Iowa, 507 pp.

White, W. B. (1995): Design of a global observing system for gyre-scale upper ocean temperature variability. *Prog. Oceanogr.*, **36**, 169–217.

White, W. B. (2000a): Coupled Rossby waves in the Indian Ocean on interannual timescales. *J. Phys. Oceanogr.*, **30**, 2972–2988.

White, W. B. (2000b): Tropical coupled Rossby waves in the Pacific ocean-atmosphere system. *J. Climate*, **30**, 1245–1264.

White, W. B. (2001): Evidence for coupled Rossby waves in the annual cycle of the Indo-Pacific Ocean. *J. Phys. Oceanogr.*, **31**, 2944–2957.

White, W. B. and J. L. Annis (2003): Diagnosing heat and vorticity budgets of annual coupled Rossby waves. *J. Phys. Oceanogr.* (in review).

White, W. B. and S.-C. Chen (2002): Thermodynamic mechanisms responsible for the troposphere response to SST anomalies in the Antarctic circumpolar wave. *J. Climate*, **15**, 2577–2596.

White, W. B. and J. F. T. Saur (1983): Sources of interannual baroclinic waves in the eastern subtropical North Pacific. *J. Phys. Oceanogr.*, **13**, 1035–1046.

White, W. B., Y. Chao and C.-K. Tai (1998): Coupling of biennial oceanic Rossby waves with the overlying atmosphere in the Pacific Basin. *J. Phys. Oceanogr.*, **28**, 1236–1251.

White, W. B., D. R. Cayan, M. Dettinger and G. Auad (2001): Sources of global warming in upper ocean temperature during El Niño. *J. Geophys. Res.*, **106**, 4349–4367.

Woodruff, S. D., S. J. Lubker, K. Wolter, S. J. Worley and J. D. Elms (1993): Comprehensive ocean-atmosphere data set release 1a; 1980–92. *Earth Systems Monitor*, **4**, 1–8.